Supporting Information

Triggering Anti-Kasha Organic Room Temperature Phosphorescence of Clusteroluminescent Materials

Jingyu Zhang,[a] *Yishan Jin,*[a] *Xinchi Lu,*[a] *Chengxi Sun,*[a] *Wei Ma,*[a] *Yuhang Li,*[a] *Longyan Zhang,*[a] *Runfeng Chen**[ab]

[a] State Key Laboratory of Flexible Electronics (LoFE) & Institute of Advanced Materials (IAM), Nanjing University of Posts & Telecommunications, 9 Wenyuan Road, Nanjing 210023, China. *E-mail: iamrfchen@njupt.edu.cn;*

[b] School of Materials Science and Engineering, Zhejiang Sci-Tech University, Hangzhou 310018, P. R. China

E-mail: iamrfchen@njupt.edu.cn;

1. Supplementary Experiments

Materials

Unless other mentioned, materials were used without further purification. Maleic anhydride (MA)，acrylamide (AM), 2,2'-azobis(isobutyronitrile) (AIBN), tetrahydrofuran (THF), 1,4-dioxane, methanol were purchased from Anergy Chemical. NaOH was from Sinopharm Group Chemical Reagent Co., LTD. AIBN is recrystallized from ethanol and then used as the free radical initiator.

Measurements

^{1}H-nuclear magnetic resonance (NMR) was measured with D_2O as solvent at Bruker AVANCE NEO 400 MHz instrument. Powder X-ray diffraction (XRD) spectra of the samples were tested with a Bruker D8 Advance diffractometer (Cu Kα: $\lambda = 1.5418$ Å) at room temperature. Fourier transform infrared spectroscopy (FTIR) was performed by PE-Spectrum Two instrument testing using potassium bromide pressure tablets. Gel permeation chromatography (GPC) was tested using an Agilent PL-GPC 220 chromatograph with water as the mobile phase at a flow rate of 0.6 mL min^{-1} to determine the number-averaged (M_n) and weight-averaged (M_w) molecular weights of the polymers. Deionized water was prepared by laboratory grade deionized water apparatus EPED-E2-10TJ. UV-vis adsorption spectra were measured by a UV-vis spectrometer (UV-3600, Shimadzu). Photographs were taken with a Nikon D9. The excitation-phosphorescence spectra were collected on a HITACHI F-4700 fluorescence spectrophotometer under ambient conditions. Steady-state photoluminescence (SSPL) spectra, steady-state excitation spectra, room-temperature phosphorescence (RTP) spectra, RTP lifetimes, organic ultralong RTP (OURTP) lifetimes, fluorescence lifetimes, phosphorescence decay images, and transient photoluminescence decay images were measured on an Edinburgh FLS 980 fluorescence spectrophotometer equipped with a xenon arc lamp (Xe900), a microsecond flash (μF900), and a picosecond pulsed light-emitting diode. Absolute total fluorescence quantum yields (PLQY) were measured on the FLS 980 device using an integrating sphere including both fluorescence and phosphorescence emission components. The phosphorescent quantum yield (PhQY) was obtained by peak-differentiation-imitating analysis.[1] High-performance liquid chromatogram (HPLC) spectra were collected by an Agilent1260 spectrometry. Wide-angle X-ray scattering (WAXS) patterns were achieved using the Xeuss 2.0 (Xenocs, France) with an incident X-ray Cu-Kα beam ($\lambda = 1.54189$ Å).

Thermogravimetric (TGA) and differential scanning calorimetry (DSC) analyses were performed on a NETZSCH DSC214 polyma with a heating rate of 5°C$\cdot$min^{-1} and a nitrogen flow rate of 50 cm$^3\cdot$min^{-1}.

Theoretical calculations

Theoretical calculations[2-3] were conducted with the following steps. Firstly, dimer, trimer, tetramer, pentamer, and hexamer containing only one MA unit were constructed to assemble the MA and AM copolymer. For example, the dimer consists of two AM units and one MA unit, while hexamer has six AM units and one MA unit. Then, the geometric optimizations of oligomers at the ground state (S_0) were performed using density functional theory (DFT) calculations, using Gaussian 09 software with the B3LYP functional and 6-31G(d) basis set. The singlet (S_1) and triplet (T_n) excited state energies were predicted using time-dependent DFT (TD-DFT) method with the B3LYP generalized 6-31G(d) basis set based on the S_0 geometry. The spin-orbit coupling (SOC) values were computed using ORCA version 5.0 software with the B3LYP generalized functional and cc-pVDZ basis set based on the optimized T_1 geometry. Nonbonding covalent interaction (NCI) analyses were adopted to investigate the intramolecular interactions using Multiwfn version 3.8. The Visual Molecular Dynamics (VMD) program was used to plot the color-filled iso-surface graphs to visualize the molecular orbitals. NCI isosurface plots with color were performed using Multiwfn version 3.8[4] software based on the B3LYP/6-31G(d) optimized molecular structures at S_0; the dark blue color represents attractive interactions, while dark red color represents repulsive interactions. All the plotted isosurfaces were demonstrated with reduced density gradient (RDG) of 0.5 and $-0.05 < \mathrm{sign}(\lambda_2)\rho < 0.05$, where sign($\lambda_2$) means the sign of the second largest eigenvalue of Hessian and ρ represents the electron density. Oscillator strength of excited states was given at TD-B3LYP/6-31G(d) level by Dalton2020.

Preparation of polyacrylamide (PAM)

In a typical procedure, AM (1.42 g, 20 mmol), 2,2'-azobis(isobutyronitrile) (AIBN, 32 mg, 0.2 mmol) were dissolved in ultra-dry tetrahydrofuran (THF, 30 mL). The solution was heated at 65°C for 12 h in an argon atmosphere. The mixed solution is poured into methanol (300 mL) and the precipitate is collected by filtration to obtain the crude polymer, which is purified by Soxhlet extraction for 12 h using acetone, petroleum ether, and dichloromethane, respectively.

Finally, the purified white polymer in powder was dried in a vacuum oven at 45°C to obtain PAM with a yield of 90%.

Preparation of poly(acrylamide-co-maleic anhydride) ($PAMMA_x$)

The copolymerization was performed in the same way of PAM using AM and MA as the monomers in varied feed ratios to afford $PAMMA_x$, where x is the molar ratio of MA and x= 0.1, 0.2, 0.5, 1, 2, and 4 mol%. Taking $PAMMA_{2\%}$ containing 2 mol% MA as an example, AM (3.55 g, 50 mmol), MA (98 mg, 1 mmol) and AIBN (83 mg, 0.51 mmol) were mixed and dissolved in ultra-dry 1, 4-dioxane (100 mL). The reaction was carried out at 75°C under an argon atmosphere for 6 h. The mixed solution was then poured into a large amount of n-hexane (1000 mL). The resulting precipitate was filtered and collected, followed by Soxhlet extraction with acetone, petroleum ether, and dichloromethane, each for 12 h. Finally, the purified white powder was dried in a vacuum oven at 45°C to obtain $PAMMA_{2\%}$ with a yield of 86%. Unless otherwise specified, $PAMMA_{2\%}$ was used as the research model in this study and for simplicity, PAMMA was used to stand for $PAMMA_{2\%}$.

Preparation of hydrolyzed PAMMA (PAMMA-h)

Typically, $PAMMA_{2\%}$ (0.36 g) was dissolved in 20 mL deionized water. Under stirring, 10 mL THF was added into the PAMMA solution slowly, followed by further stirring at room temperature for 1 h. The mixed solution was heated in an oven at 60°C to remove all the solvents, affording a transparent polymer film of PAMMA-h.

Preparation of ionic PAMMA (PAMMA-Na, PAMMA-Ca, PAMMA-Ba)

Due to the high reactivity of the anhydride group, which can be easily hydrolyzed in an alkaline environment, the PAMMA polymer undergoes hydrolysis upon the addition of NaOH to form the ionized polymer PAMMA-Na. Typically, $PAMMA_{2\%}$ (0.73 g, containing 0.2 mmol MA unit) and NaOH (0.016 g, 0.4 mmol) were dissolved in 50 mL deionized water and stirred at 60°C for 12 h. The resulting transparent solution was then placed in an oven at 60°C for 12 h to remove all the solvents. Finally, a transparent ionized $PAMMA_{2\%}$ film with Na^+ was obtained, and the yield is over 95%. Considering using 2 equivalent NaOH compared to the MA unit, the full ionization will be resulted and the obtained polymer is named as $PAMMA_{2\%}$-$Na_{100\%}$. Also, other $PAMMA_x$ can be similarly ionized, and the degree of ionization (y) can be controlled by adjusting the equivalent ratio of NaOH to MA unit in copolymer, leading to various PAMMA$_x$-Na$_y$ (y=50, 75, and 100%). Since PAMMA$_{2\%}$-Na$_{100\%}$ has the optimal photophysical property as found in the main text, it was simplified to PAMMA-Na. The ionized PAMMA-Ca and PAMMA-Ba polymers, which contain Ca^{2+} and Ba^{2+}, were prepared in an identical procedure to that of PAMMA-Na, by replacing NaOH with $Ca(OH)_2$ and $Ba(OH)_2$.

Preparation of PAMMA-H

Typically, PAMMA$_{2\%}$-Na$_{100\%}$ (0.183 g) was dissolved in 25 mL of deionized water and stirred until the polymer was completely dissolved. Then, 0.4 mg hydrochloric acid was added into the solution and the temperature was raised to 60°C for continuous stirring of 12 h. The solution was transferred to a 60°C oven to remove all the solvents, resulting in a transparent polymer film of PAMMA-H.

Temperature-dependent "heart/lock" shaped pattern encryption

The temperature and lifetime encrypted pattern was fabricated in a two-step silk screen printing process. Firstly, PAMMA and PAMMA-Na were separately dissolved in deionized water to prepare their solutions with a concentration of 1 g/mL. Secondly, on an A4 paper substrate, the PAMMA and PAMMA-Na solutions were used to print heart and lock patterns, respectively. Subsequently, the paper was dried at 70°C for 12 h to obtain a transparent "heart/lock" shaped pattern. At room temperature, the heart/lock pattern exhibits green OURTP when the UV light is switched off. After being frozen in a -24°C refrigerator, the lock pattern appears in a blue OURTP originated from PAMMA-Na.

Multi-level information encrypted word

PAM, PAMMA, and PAMMA-Na were dissolved in deionized water to prepare their solutions with a concentration of 0.1 g/mL, respectively. The prepared solutions were subsequently used as inks to write a word on A4 paper with a brush. Then, the paper was dried at 70°C for 12 h to obtain the multi-level encrypted word.

3D RTP model

PAMMA-Na solution with a concentration of 1 g/mL is poured into the various molds. After being dried in a 70°C oven for 12 h, these 3D RTP models in different shapes were obtained after demolding.

Synthetic route

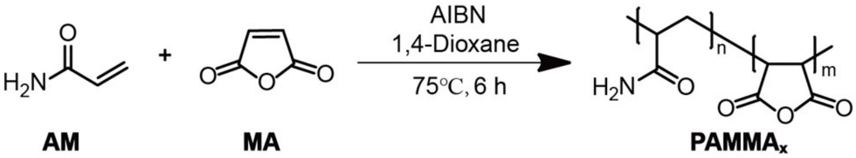

Scheme S1. Synthesis of PAMMA$_x$.

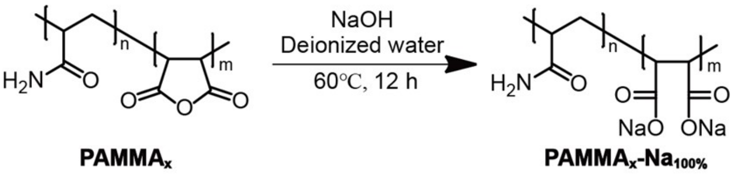

Scheme S2. Synthesis of PAMMA$_x$-Na$_{100\%}$.

2. Supplementary Figures and tables

Table S1. Summary of anti-Kasha RTP materials and their emission peaks.

Material	S_1 (nm)	T_n (nm)	T_1 (nm)	Blue-shift [a] (nm)	Red-shift [b] (nm)	Reference
1-PhB-0.1%	437	424	483	13	-	[3]
DPPZ	440	480	575	-	40	[5]
SDPE-OO	451	453	548	-	2	[6]
ClBDBT	467	467	570	-	-	[7]
triamino-s-triazine	345	464	649	-	121	[8]
diphenylsulfone	325	425	490	-	100	[9]
PAMMA-Na	**428**	**399**	**488**	**29**	**-**	**This work**

Note: S_1, T_n, and T_1 represent the lowest singlet excited state, the high-lying triplet excited state, and the lowest triplet excited state, respectively;

a and b represent the blue and red-shifted emission peaks of T_n compared to S_1, respectively.

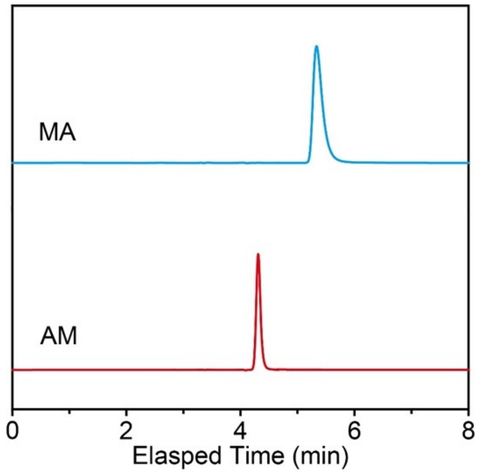

Figure S1. HPLC of MA and AM monitored at the onset absorption of 220 nm. MA and AM were collected in methanol-1% phosphoric acid solution (v/v, 2/98) and acetonitrile-water (v/v, 2/98), respectively.

Table S2. Molecular structure characterizations of PAMMA$_x$ (x=0.1, 0.2, 2, and 4 mol%).

Materials	MA in feed (mol%)	MA in polymer (mol%)	M_n	M_w	M_w/M_n
PAMMA$_{4\%}$	4	4.2	5229	14549	2.78
PAMMA$_{2\%}$	2	2.0	8206	26298	3.20
PAMMA$_{0.2\%}$	0.2	0.2	7958	40498	5.09
PAMMA$_{0.1\%}$	0.1	0.1	7030	24684	3.51

Note: MA content in polymer was calculated from ^{1}H NMR spectrum based on the integration areas of the characteristic hydrogen protons of AM (1.64-2.32 ppm) and MA (3.75 ppm) units.

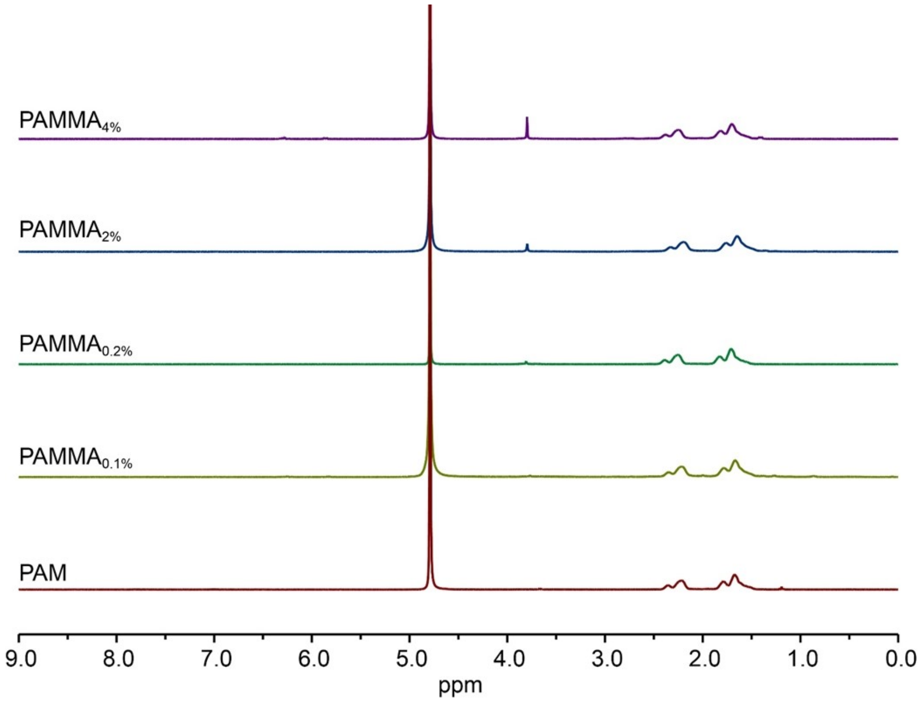

Figure S2. ^{1}H NMR spectra of PAM and PAMMA$_x$ (x=0.1, 0.2, 0.5, 1, 2, and 4 mol%) in D_2O.

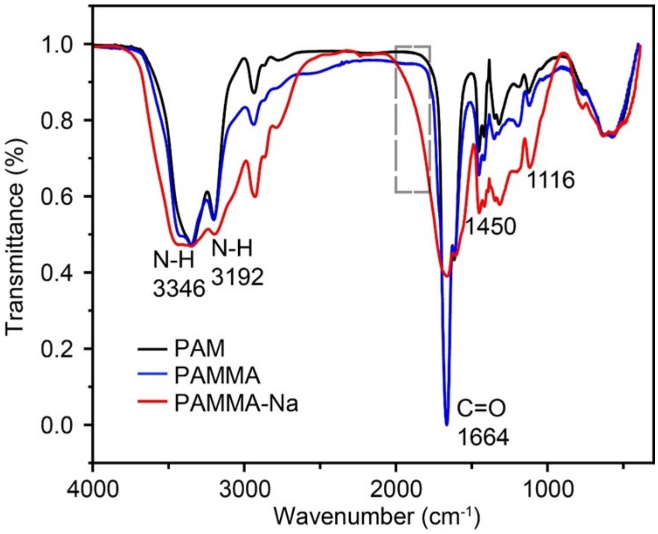

Figure S3. FTIR spectra of PAM, PAMMA, and PAMMA-Na.

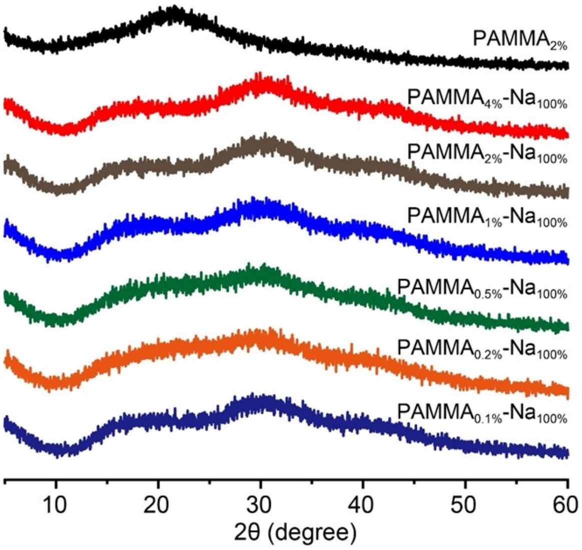

Figure S4. Powder XRD patterns of PAMMA and PAMMA$_x$-Na$_{100\%}$ (x=0.1, 0.2, 0.5, 1, 2, and 4 mol%) in film.

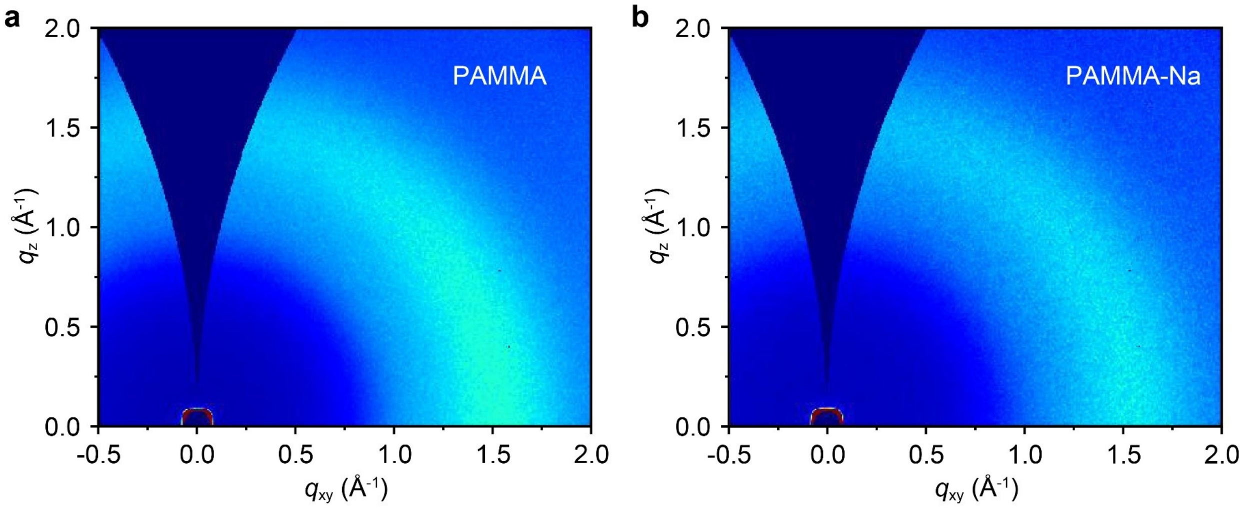

Figure S5. WAXS patterns of (a) PAMMA and (b) PAMMA-Na films.

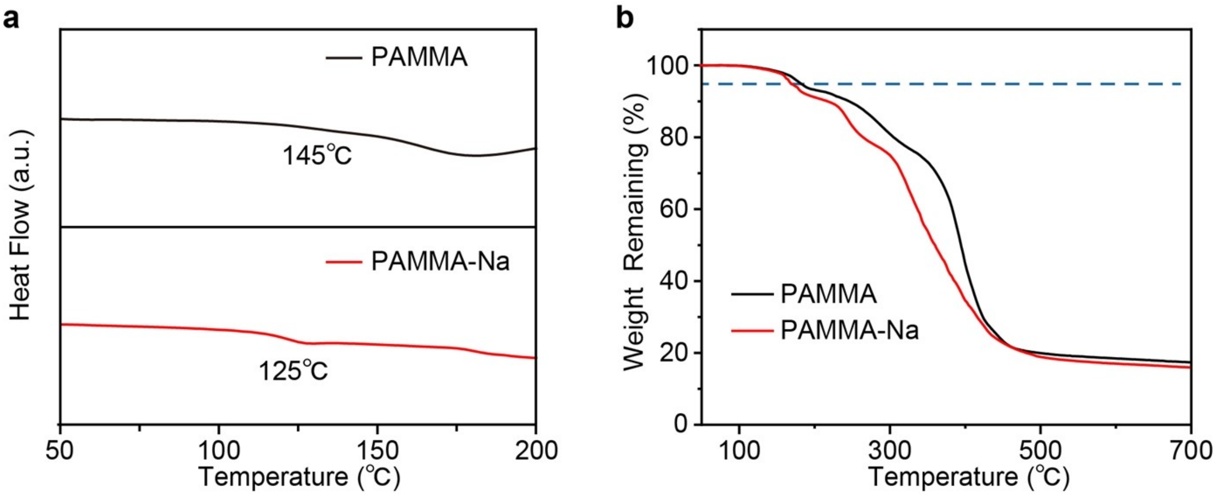

Figure S6. (a) DSC and (b) TGA curves of PAMMA and PAMMA-Na films.

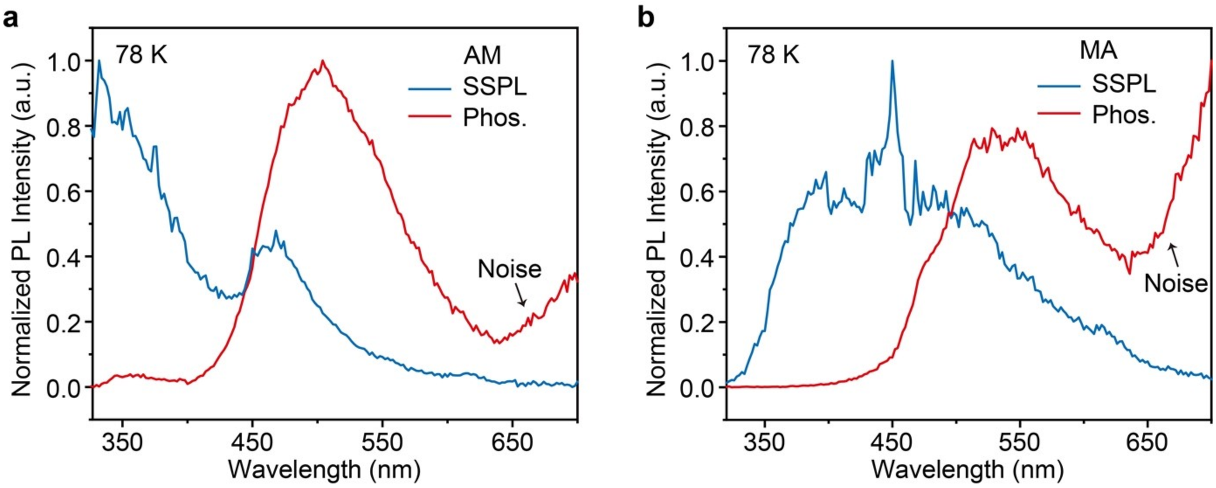

Figure S7. Normalized SSPL spectra and phosphorescence spectra of (a) AM and (b) MA powders at 78 K.

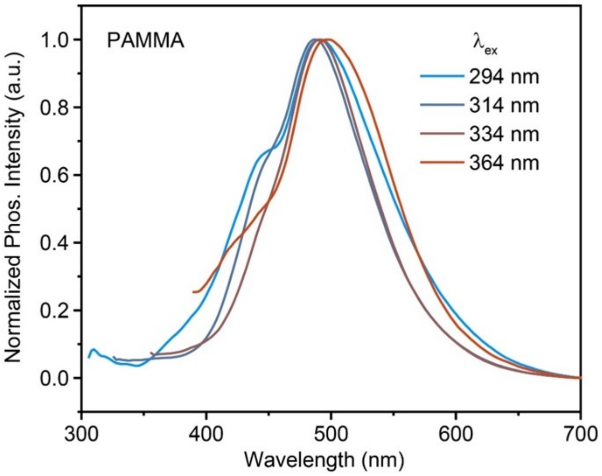

Figure S8. Phosphorescence spectra of PAMMA film at different excitation wavelengths (λ_{ex}).

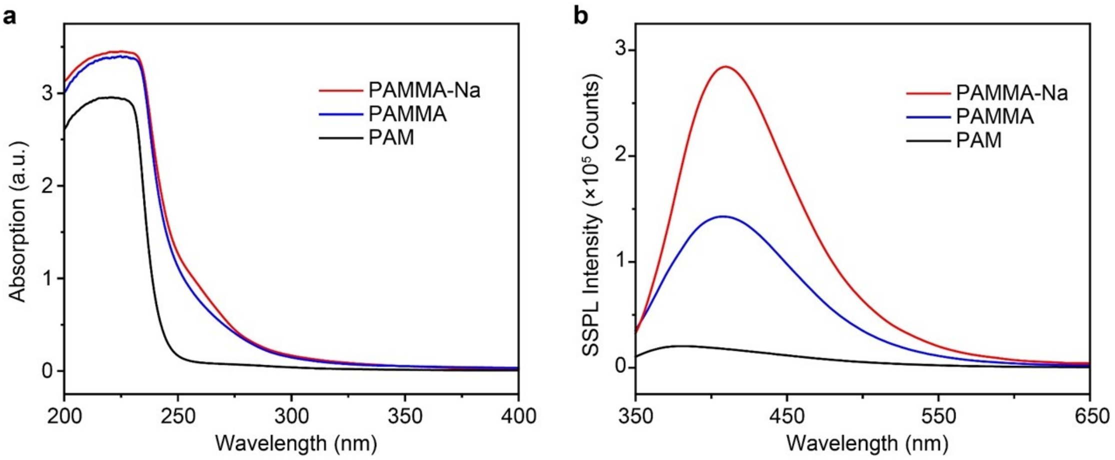

Figure S9. (a) Absorption and (b) SSPL spectra of PAM, PAMMA and PAMMA-Na in aqueous solution (both of them have a concentration of 10 mg/mL).

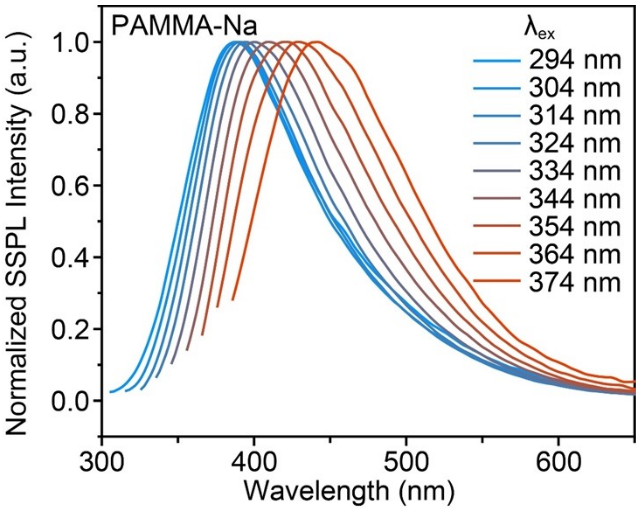

Figure S10. Excitation wavelength-dependent SSPL spectra of PAMMA-Na film at different excitation wavelengths from 294 to 374 nm.

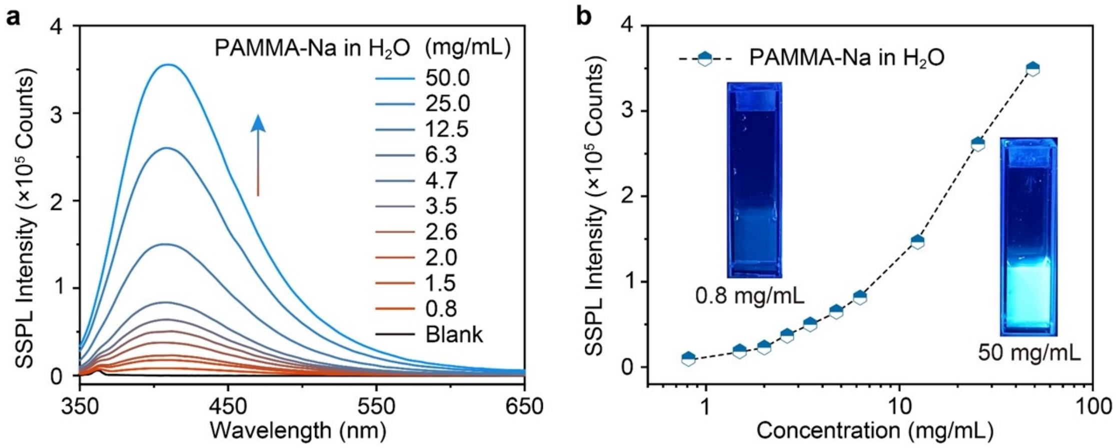

Figure S11. (a) Concentration-dependent SSPL spectra and (b) maximum intensity changes around 408 nm of PAMMA-Na in aqueous solution at different concentrations ranging from 0.8 to 50 mg/mL. Insets show the fluorescence photographs of PAMMA-Na in aqueous solution at concentrations of 0.8 and 50 mg/mL, respectively.

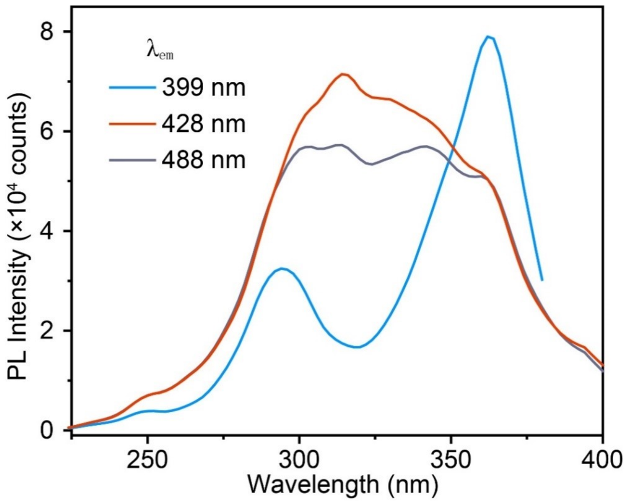

Figure S12. Excitation spectra of PAMMA-Na film monitored at the emission (λ_{em}) of RTP (399 and 488 nm) and SSPL (428 nm) peaks**.**

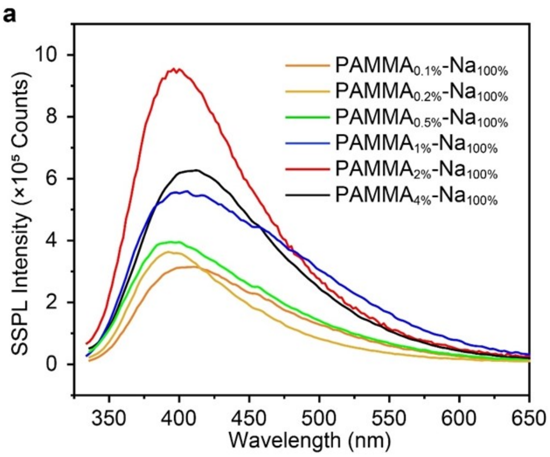

Figure S13. (a) SSPL and (b) phosphorescence (488 nm) decay curves of PAMMA$_x$-Na$_{100\%}$ (x=0.1, 0.2, 0.5, 1, 2, and 4 mol%) in film.

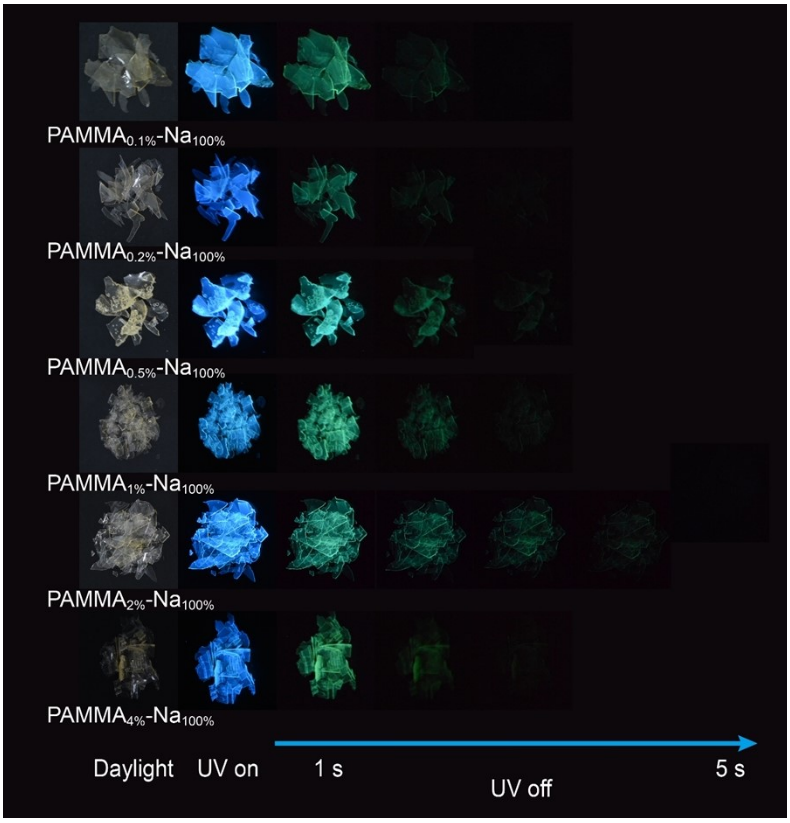

Figure S14. OURTP photographs of PAMMA$_x$-Na$_{100\%}$ (x=0.1, 0.2, 0.5, 1, 2, and 4 mol%) flakes at room temperature.

Table S3. Photophysical properties of PAMMA$_x$-Na$_{100\%}$ (x=0.1, 0.2, 0.5, 1, 2, and 4 mol%) in film.

Material	PLQY	PhQY	Lifetime (ms)
PAMMA$_4$-Na$_{100\%}$	11.2%	7.4%	312
PAMMA$_2$-Na$_{100\%}$	13.5%	8.9%	420
PAMMA$_1$-Na$_{100\%}$	13.4%	8.8%	374
PAMMA$_{0.5}$-Na$_{100\%}$	11.7%	7.7%	282
PAMMA$_{0.2}$-Na$_{100\%}$	10.2%	6.7%	259
PAMMA$_{0.1}$-Na$_{100\%}$	9.5%	6.2%	235

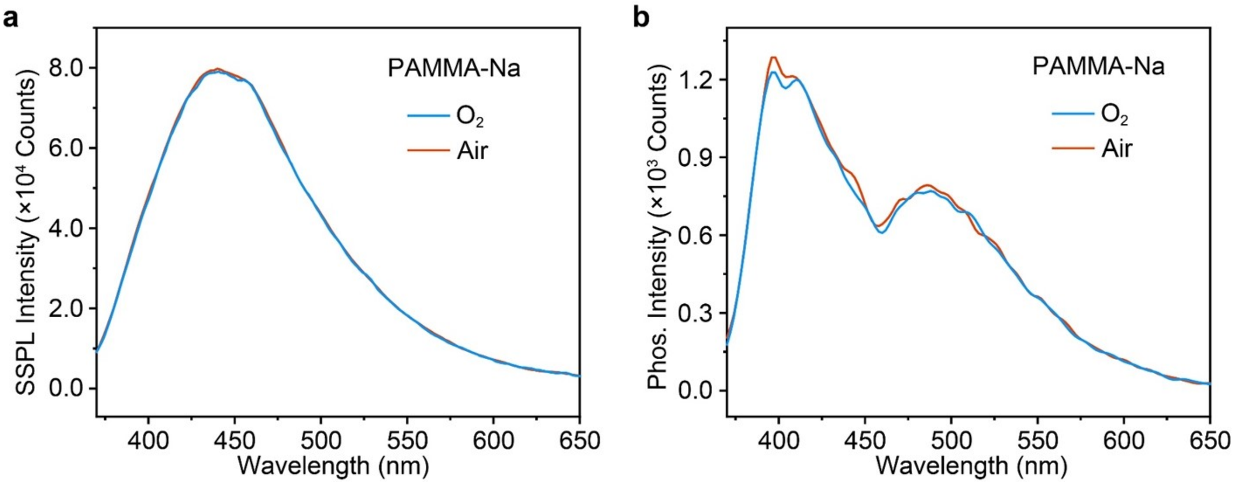

Figure S15. (a) SSPL and (b) RTP (delay 10 ms) spectra of PAMMA-Na film in O_2 and air.

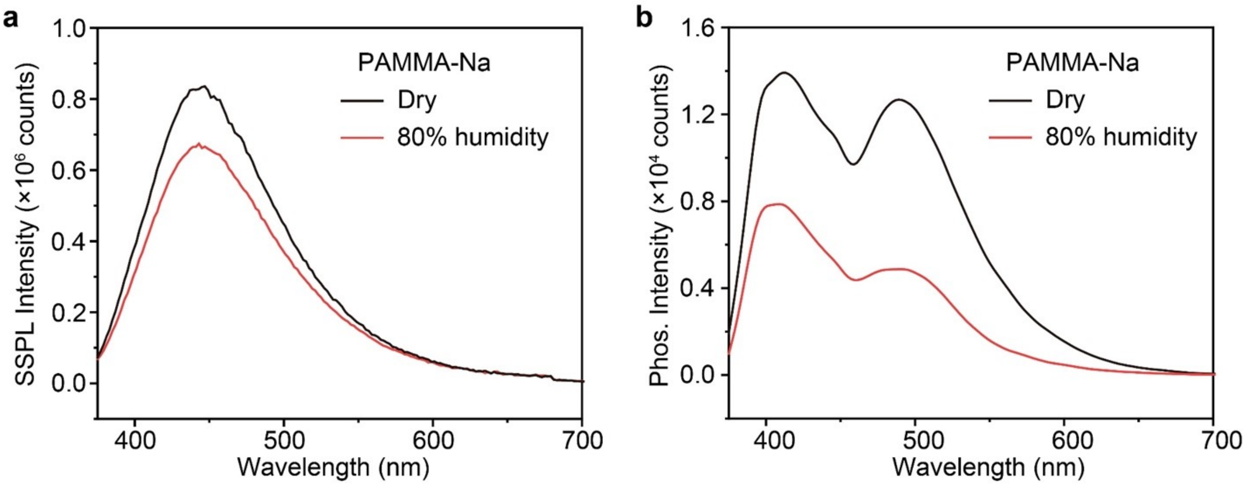

Figure S16. (a) SSPL and (b) RTP (delay 10 ms) spectra of PAMMA-Na film under dry and 80% humidity conditions.

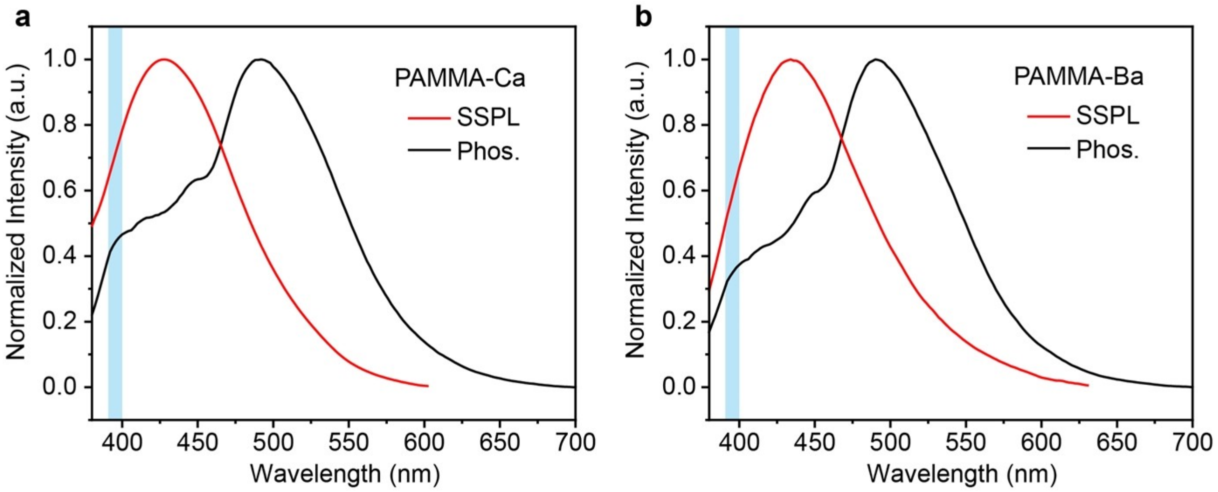

Figure S17. Normalized SSPL spectra and phosphorescence (Phos.) emission spectra of (a) PAMMA-Ca and (b) PAMMA-Ba films excited at 365 nm.

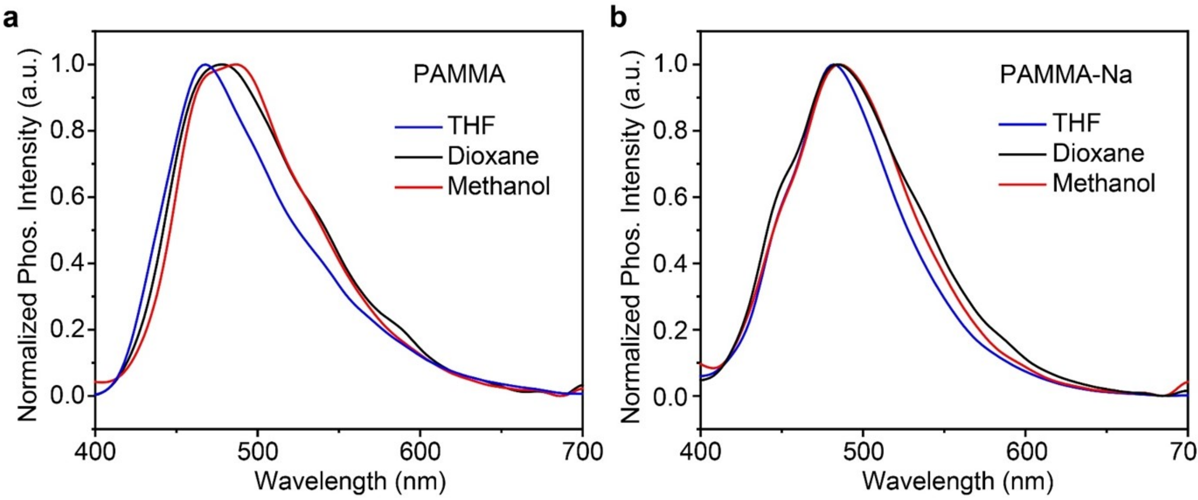

Figure S18. Normalized phosphorescence spectra of (a) PAMMA and (b) PAMMA-Na in different solvents of THF, dioxane, and methanol at 78 K.

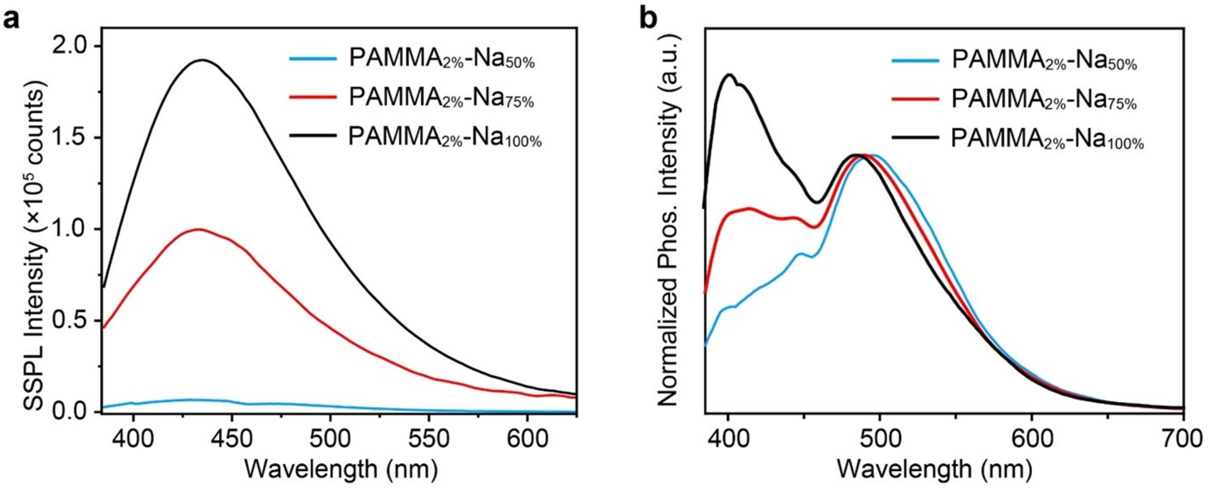

Figure S19. (a) SSPL and (b) phosphorescence (delay 10 ms) spectra of PAMMA$_{2\%}$-Na$_y$ (y=50, 75, and 100%) film at room temperature.

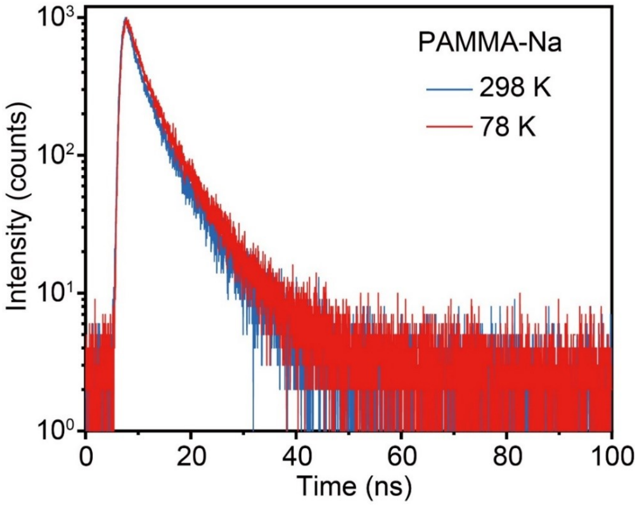

Figure S20. Prompt decay curves of PAMMA-Na film monitored at 428 nm at both 298 K and 78 K.

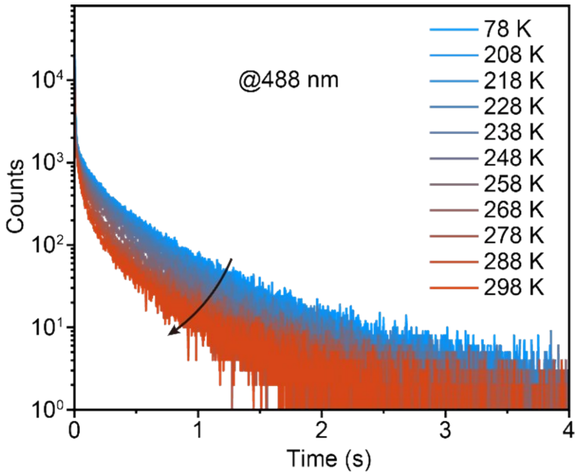

Figure S21. OURTP decay curves of PAMMA-Na film monitored at 488 nm at different temperatures.

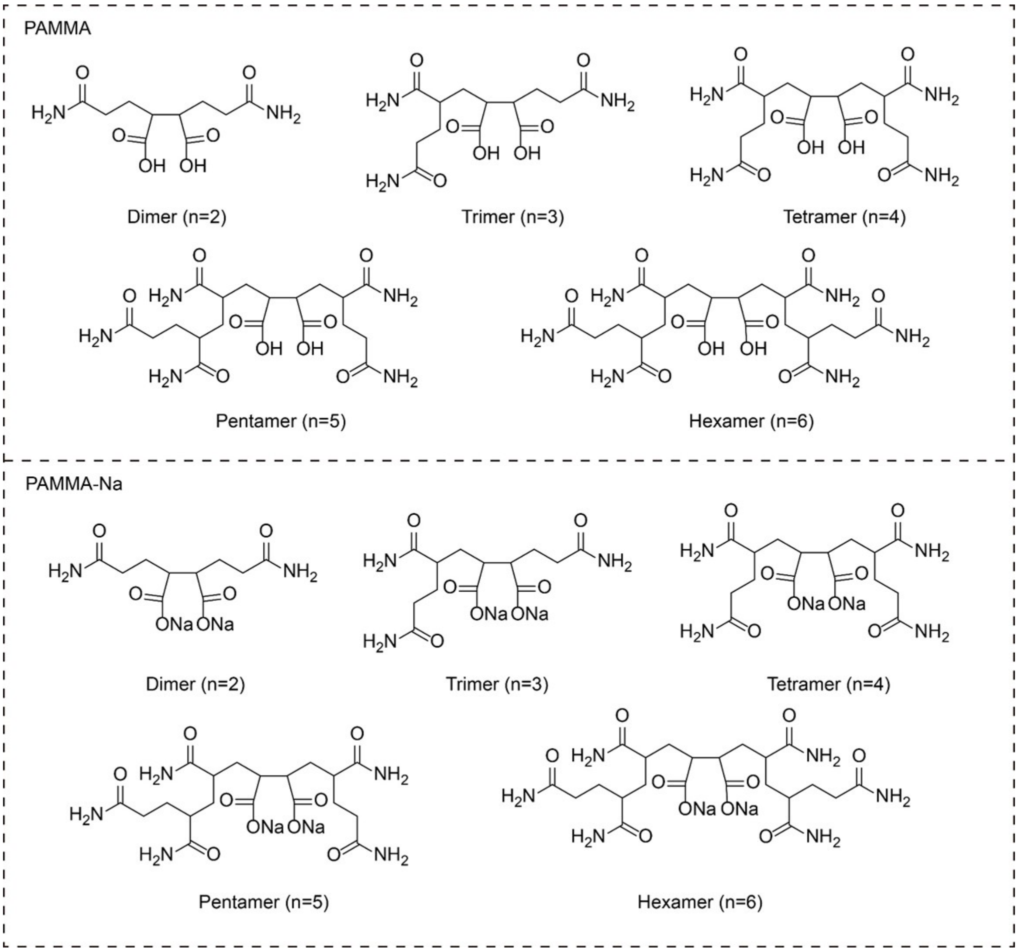

Figure S22. Oligomers with different numbers of AM (n) used to simulate the properties of PAMMA and PAMMA-Na.

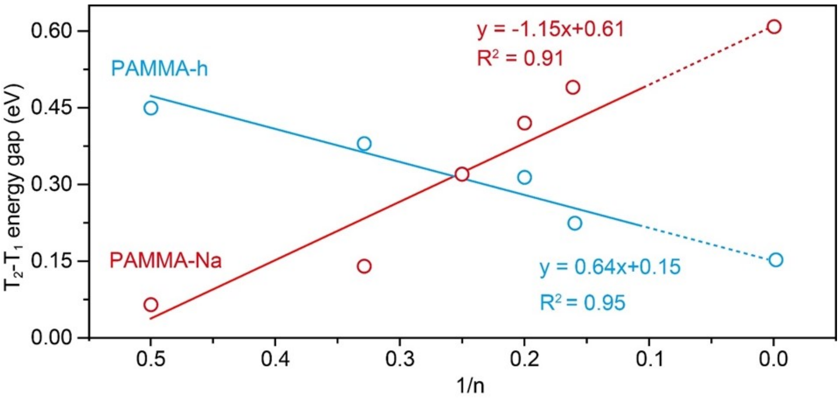

Figure S23. Theoretically predicted T_2-T_1 energy gaps of PAMMA-h and PAMMA-Na from the linear exploration of oligomers (n = 2~6), where n is the polymerization degree. When n=∞, i.e. 1/n=0, the T_2-T_1 energy gaps of the polymers can be deduced.

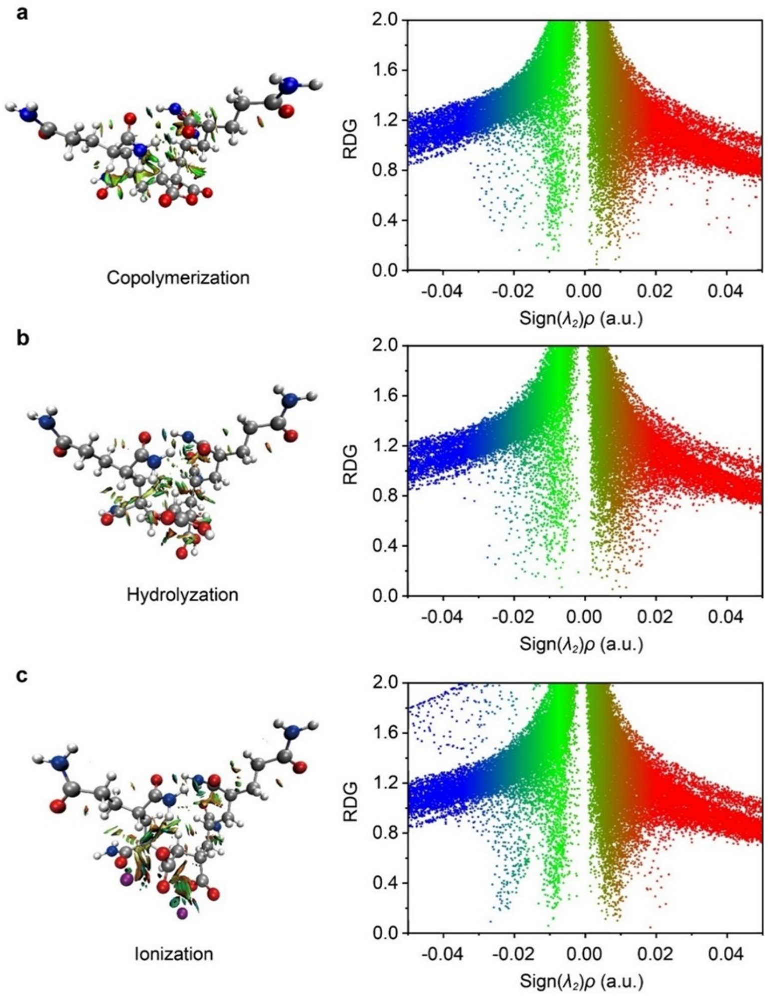

Figure S24. RDG versus sign(λ_2)ρ with the view of the RDG isosurface of the MA and AM hexamer after (a) copolymerization, (b) hydrolyzation, and (c) ionization.

Table S4. Calculated singlet-triplet splitting energy ($\Delta E_{(S1,Tn)}$) and SOC value $<S_1|\hat{H}_{SOC|}T_n>$ between S_1 and T_n energy level of PAMMA-h and PAMMA-Na from their hexamers.

	Excited state	Excited state energy (eV)	$\Delta E_{(S1,Tn)}$ (eV)	$<S_1|\hat{H}_{SOC}|T_n>$
PAMMA-h	S_1	5.08	-	-
	T_1	4.73	0.35	0.34
	T_2	4.96	0.12	0.72
PAMMA-Na	S_1	3.70	-	-
	T_1	3.66	0.16	8.82
	T_2	4.15	0.45	25.07

Table S5. Calculated oscillator strength for the RTP emission of the hydrolyzed and ionized hexamers.

	Hydrolyzed hexamer		Ionized hexamer	
	T_1-S_0	T_2-S_0	T_1-S_0	T_2-S_0
Oscillator strength	4.43×10^{-7}	6.28×10^{-8}	5.08×10^{-6}	4.18×10^{-7}

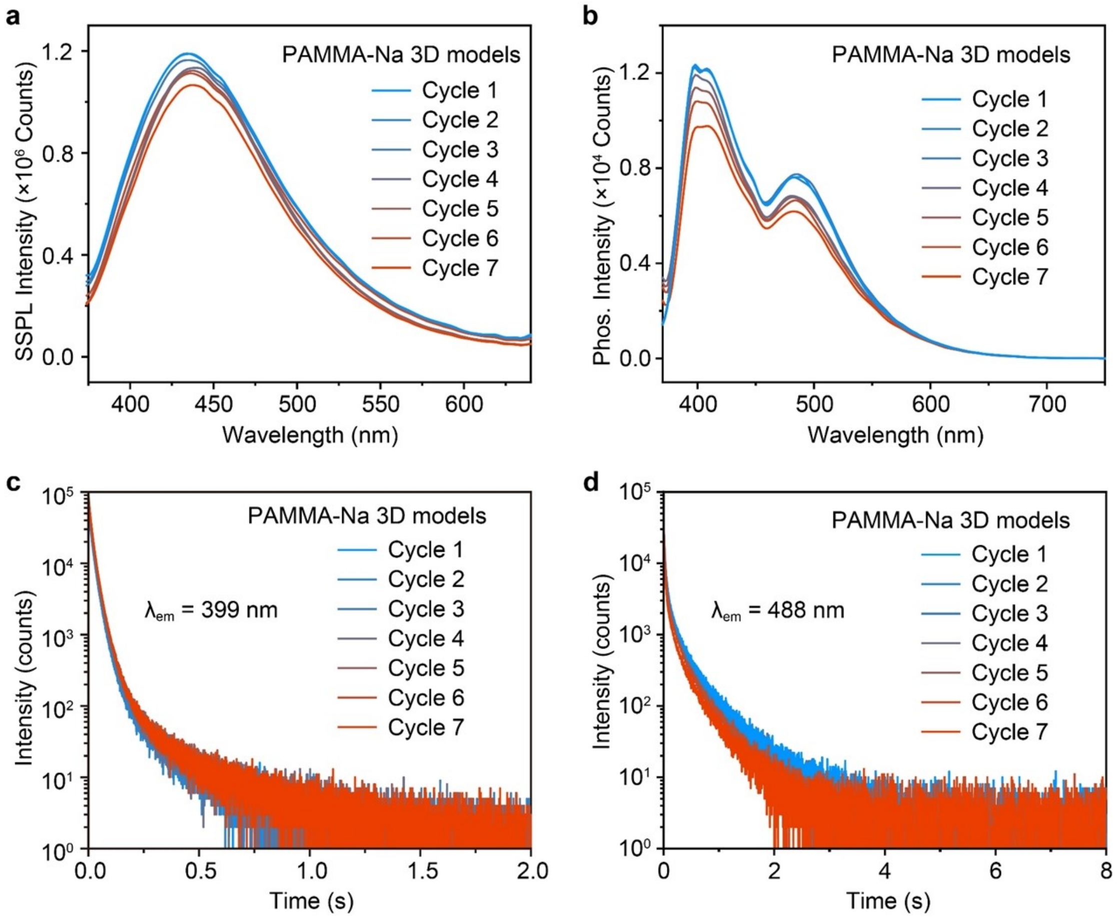

Figure S25. (a) SSPL spectra, (b) phosphorescence spectra, and (c-d) phosphorescence decay curves monitored at (c) 399 and (d) 488 nm emissions of PAMMA-Na 3D models conducted in seven solution-molding cycles.

Reference

[1] W. Ye, H. Ma, H. Shi, H. Wang, A. Lv, L. Bian, M. Zhang, C. Ma, K. Ling, M. Gu, Y. Mao, X. Yao, C. Gao, K. Shen, W. Jia, J. Zhi, S. Cai, Z. Song, J. Li, Y. Zhang, S. Lu, K. Liu, C. Dong, Q. Wang, Y. Zhou, W. Yao, Y. Zhang, H. Zhang, Z. Zhang, X. Hang, Z. An, X. Liu, W. Huang, *Nat. Mater.* **2021**, *20*, 1539-1544.

[2] Q. Mu, K. Zhang, H. Zou, H. Liu, Y. Song, C.-K. Wang, L. Lin, J. Fan, *Dyes and Pigments* **2022**, *205*, 110560.

[3] J. Li, X. Li, G. Wang, X. Wang, M. Wu, J. Liu, K. Zhang, *Nat. Commun.* **2023**, *14*, 1987.

[4] C. Lefebvre, G. Rubez, H. Khartabil, J.-C. Boisson, J. Contreras-García, E. Hénon, *Phys. Chem. Chem. Phys.* **2017**, *19*, 17928-17936.

[5] C. Zhou, S. Zhang, Y. Gao, H. Liu, T. Shan, X. Liang, B. Yang, Y. Ma, *Adv. Funct. Mater.* **2018**, *28*, 1802407.

[6] Y. H. Wu, H. Xiao, B. Chen, R. G. Weiss, Y. Z. Chen, C. H. Tung, L. Z. Wu, *Angew. Chem. Int. Ed.* **2020**, *59*, 10173-10178.

[7] Z. He, W. Zhao, J. W. Y. Lam, Q. Peng, H. Ma, G. Liang, Z. Shuai, B. Z. Tang, *Nat. Commun.* **2017**, *8*, 416.

[8] Q. S. Zhang, S. C. Wang, X. H. Xiong, P. Y. Fu, X. D. Zhang, Y. N. Fan, M. Pan, *Angew. Chem. Int. Ed.* **2022**, *61*, e202205556.

[9] W. Xie, W. Huang, J. Li, Z. He, G. Huang, B. S. Li, B. Z. Tang, *Nat. Commun.* **2023**, *14*, 8098.